Temporary Cover

AIAA 2003-xxxx

Title: Comparison of Experimental Data and Computations Fluid Dynamics Analysis for a Three Dimensional Linear Plug Nozzle

Authors:
J. H. Ruf
NASA Marshall Space Flight Center,
Applied Fluid Dynamics Analysis Group
Huntsville, AL USA

G. Hagemann
Astrium GmbH, Space Infrastructure Division,
Munich, Germany

H. Immich
Astrium GmbH, Space Infrastructure Division,
Munich, Germany

39th AIAA/ASME/SAE/ASEE
Joint Propulsion Conference and Exhibit
July 2003, Huntsville, Alabama

Abstract

A three dimensional linear plug nozzle of area ratio 12.79 was designed by EADS Space Transportation (former Astrium Space Infrastructure). The nozzle was tested within the German National Technology Program 'LION' in a cold air wind tunnel by TU Dresden. The experimental hardware and test conditions are described. Experimental data was obtained for the nozzle without plug side wall fences at a nozzle pressure ratio of 116 and then with plug side wall fences at NPR 110. Schlieren images were recorded and axial profiles of plug wall static pressures were measured at several spanwise locations and on the plug base. Detailed CFD analysis was performed for these nozzle configurations at NPR 116 by NASA MSFC. The CFD exhibits good agreement with the experimental data. A detailed comparison of the CFD results and the experimental plug wall pressure data are given. Comparisons are made for both the without and with plug side wall fence configurations. Numerical results for density gradient are compared to experimental Schlieren images. Experimental nozzle thrust efficiencies are calculated based on the CFD results. The CFD results are used to illustrate the plug nozzle fluid dynamics. The effect of the plug side wall is emphasized.

Nomenclature

M, Mach number
p, pressure
T, temperature
K, Kelvin
x, axial station
y, vertical coordinate
z, spanwise station

Subscripts

a, absolute
c, chamber or total pressure
c,total chamber or total pressure
D, design
in, inlet
id, internal design
w, wall

Abbreviation

CFD, Computational Fluid Dynamics
EADS, European Aeronautic Defence and Space Company
ESA, European Space Agency
ESTEC, European Space Research and Technology Center
FESTIP, Future European Space Transportation Investigation Program
FOI, Swedish Defense Research Agency
HWK,
LION, Linear Internal / External Optimized Plug Nozzle Program
LPNI, Linear Plug Nozzle Investigation
MSFC, Marshall Space Flight Center
NASA, National Aeronautics and Space Administration
NATO, North Atlantic Treaty Organization
NPR, Nozzle Pressure Ratio
ONERA, Office of National Studies and Aerospace Research
RTO, Research and Technology Organization
SRPT, Surface Restricted Particle Traces
TRP,
TU Dresden, Technical University of Dresden

Introduction

In 1995 a first experimental and numerical investigation on linear plug nozzles was initiated in Europe within the framework of the ESA Program, FESTIP. The objectives of the test were to achieve a

basic understanding of the flow phenomena and to gain insight into performance of the linear plug concept. Tests were conducted under different pressure ratios corresponding to sea level operation up to high altitude operation. These first tests on linear plug nozzles indicated that improved contour design methods should be developed, particularly for plug nozzles with a portion of the expansion occurring internally. Within the follow-up LION program, improved contour design methods were developed and verified by additional cold gas nozzle tests. Hagemann, et al [1] summarizes these activities dedicated to establishing contour design methods for plug nozzle configurations with both internal and external expansion. Figure 1 illustrates the plug geometry used for further cold gas nozzle tests. In Figure 2 the plug nozzle hardware is shown mounted inside the wind tunnel of TU Dresden.

Within the framework of the NATO RTO Working Group 10, the Plug Nozzle Subgroup worked on two main objectives regarding aerothermodynamics and performance of plug nozzles: i) develop a thorough understanding of the fluid dynamics of plug nozzles, and ii) assess the ability of modern CFD codes to capture the fluid dynamics of plug nozzles. This second objective involved three steps; defining relevant CFD test cases, conducting the CFD simulations of the test cases, and comparing CFD results with experimental data. The three test cases were:

1. Full length annular plug nozzle, designed and tested by ONERA.
2. Truncated annular plug nozzle, tested by FOI.
3. LION, a truncated linear plug nozzle with combined internal and external expansion, designed and tested by EADS Space Transportation.

In the Plug Nozzle Subgroup, different institutes, organizations, and companies within Europe and the US were asked to perform numerical simulations on the defined test cases. Each participant was supplied with test case geometry and boundary conditions. Experimental data sets were not provided in advance. Therefore, each numerical simulation was a true prediction of the nozzle flowfield development. In total, nine different numerical schemes were applied to the test cases, producing about 20 different numerical simulations of the test cases. Findings and conclusions for all test cases are summarized in Reference 2.

Specific numerical results by NASA/MSFC for the LION test hardware are discussed in this paper. In addition to the LION test case summarized in Reference 2, and additional benchmark calculation was performed on a LION configuration with side fences added to the plug nozzle. This paper summarizes the results established within this cooperation between NASA/MSFC and EADS Space Transportation.

Experiment

Nozzle Design and Test Hardware

Within the LION program, a truncated ideal nozzle was chosen for the primary or internal expansion. Figure 3 illustrates the principle of the developed design approach. The exhaust flow initially expands in the symmetric internal expansion nozzle from the throat area AB to the internal exit area DE. Due to the truncated design, the exhaust flow is not uniform, but has the internal design Mach number M_{id} in the core. At the point F on the plug contour, this Mach number M_{id} is settled. The contour segment DF is of special type being designed with the method of characteristics along which the initially non-homogeneous exit flow is homogeneously expanded exactly to M_{id}. The further contour FG is defined following again the classical way with the method of characteristics.

For the plug side fence, a constant height of half of the module exit height was found to be sufficient to fully avoid any parasitic expansion in span wise direction. Further information on the chosen design approach, and also on other approaches is included in Reference 1.

Facility and Test Point Flow Conditions

Cold gas tests with the plug nozzle hardware were performed for various pressure ratios at the HWK wind tunnel of Technical University of Dresden located at Merkers. Design data for the testing are summarized in Reference 1. Figure 2 shows the hardware mounted inside the wind tunnel test cell.

The plug nozzle test article has been tested in three different truncated configurations. The configuration with the longest central plug body truncated at 39.3% of its ideal length was selected as reference configuration for the further CFD assessment. Two different flow conditions have been selected. The prescribed flow conditions to be assumed for the numerical simulations were:

Flow condition #1, without side fences:

- Pressure ratio $p_{c,total}/p_a$: 116
- Feeding chamber stagnation temperature, $T_{c,total}$: 293 K
- Test chamber temperature, T_a: 293 K

Flow condition #2, with side fences:

- Pressure ratio $p_{c,total}/p_a$: 110
- Feeding chamber stagnation temperature, $T_{c,total}$: 293 K
- Test chamber temperature, T_a: 293 K

Computational Approach

Code and Solver Process

The CFD code used in this analysis was FDNS [3]. It is a general purpose, multidimensional, multi-species, viscous flow, pressure-based reacting flow solver. FDNS solves the Reynolds-averaged transport equations with a variety of options for physical models and boundary conditions. To solve the system of nonlinear partial differential equations, the code uses finite-difference approximations to establish a system of linearized algebraic equations. Several difference schemes were employed to approximate the convective terms of the momentum, energy and continuity equations, including central difference [3], upwind and total-variation-diminishing schemes [4]. Viscous fluxes and source terms are discretized using a central-difference approximation. A pressure-based predictor plus multiple-corrector solution method is employed so that flow over a wide speed range (from low subsonic to supersonic) can be analyzed.

Both standard and extended two-equation turbulence model [5] closure can be used to describe the turbulent flow. The compressibility effect on the turbulence is taken into account by the method of Mach-number correction. A modified wall function approach [6] is employed by incorporating a complete velocity profile [7]. This complete velocity profile provides a smooth transition between Logarithmic law-of-the-wall and linear viscous sublayer velocity distributions. Further details of the numerical methodology are given in Reference 3.

The plug nozzle calculations discussed in this paper were solved steady state, implementing the second order central scheme and an extended two-equation k-ε turbulence model.

Mesh and Boundary Conditions

The computational domain modeled one-quarter of the three dimensional test hardware, as shown in the top of Figure 4, with two separate meshes. The first mesh mapped the internal expansion, or 'thruster'. The second mesh, shown in Figure 4, mapped the external expansion domain. The two meshes match identically at their interface: the exit of the thruster, the red mesh in Figure 4, was also an inlet to the external domain.

The thruster mesh contained 8e+5 nodes. Its boundary conditions were no-slip adiabatic on the walls, a symmetry plane at z=0, a subsonic fixed mass flow inlet and a supersonic exit. The external mesh contained 4.6e+6 nodes. It included far-field regions upstream, outboard and above the nozzle. The domain was sufficiently wide outboard of the nozzle to capture the lateral spillage of the plume. The same mesh was used to model the 'without-fence' and 'with-fence' test configurations. The fence geometry, shown by the black mesh at the edge of the plug in Figure 4, was embedded in the domain. To model the with fence condition, the region of the mesh that represented the fence was designated a no-slip wall. For the without-fence configuration this region was simply part of the mesh volume.

The external domain boundary conditions were no-slip adiabatic on the walls, symmetry planes at y=0 and z=0 planes and an exit at the downstream boundary. Far-field boundary conditions were applied to

faces upstream, outboard and above the nozzle. The free stream flow properties were initialized as quiescent with a static pressure to match the test conditions described above.

The total conditions for the CFD where similar to the experimental work but not exactly the same. Both the without- and with-fence plug configurations were calculated at NPR 116. The experimental data was measured at NPR 116 and NPR 110, respectively. Therefore, all comparisons are made via nondimensional curves.

The mesh presented here produced mesh independent solutions.

Results: 3D CFD Compared to Experimental Data

In the following section both the experimental data and CFD results for the plug nozzle configuration without the plug side wall fences are for NPR 116. For the with-fence configuration, the experimental data was taken at NPR 110 and the CFD results were calculated at NPR 116.

Schlieren

Figure 5 compares the experimental Schlieren for the without-fence configuration to the density gradient from the CFD solution. This experimental Schlieren image for NPR 116 was produced in a test prior to the NPR 110 data presented in this paper. Both halves Figure 5 are for NPR 116 but present slightly different data. In the experimental image the light source passed through the entire width of the plume so the three dimensional effects are present to some extent in the Schlieren. The CFD half of the image, however, is a two-dimensional slice from the centerline of the three dimensional solution. Never-the-less, the position of all major plume features agree well. They agree on the shear layer, the barrow shock, the kernel of the initial thruster expansion region, the plug base recirculation size and the shock structure in the plug base.

Experimental Wall Pressure

Figure 6 illustrates the experimental plug wall pressure distribution measured with 82 static pressure taps through Scanivalves for both configurations. For the without-fence configurations the effect of the lateral expansion, mainly driven by inviscid effects, resulted in the lower pressures along the edges of the plug. The relatively constant pressure distribution of the with-fence configuration indicates the fences effectively eliminated the lateral expansion effects on the plug pressures.

CFD Flow Visualization

Figure 7 illustrates several flow features of NPR 116 without-fence configuration. In this figure the exit plane of the thruster and the plug walls are colored by static pressure, surface restricted particle traces are shown in black and particle flow paths outboard of the plug are shown as yellow ribbons. The lateral expansions of the plume off the plug, or 'plume spillage', is evident in the SRPT movement toward the edge of the plug. It is also evident in the curved shape of the pressure contours near the edge of the plug. The additional lateral expansion, due to the spillage, resulted in lower wall pressure near the edge of the plug relative to its centerline. Note that the character of the pressure gradients in this CFD result are very similar to the experiment results shown in Figure 6. Both the SRPT and pressure contours show the plume spillage effects penetrating further inward as the flow progresses down the plug.

A recirculation on the plug base outboard edge is clearly illustrated with the SRPT and particle ribbons. In the CFD solution, the pressure in this region of the plug base is less than ambient resulting in the flow recirculation shown.

Figure 8 shows the same graphics techniques illustrating the flow features of NPR 116 with-fence configuration. The fence is visible on the edge of the plug. It is shown with the color contours of pressure that exist on the inboard side but with the SRPT from its outboard side. The pressure contours and SRPT on the plug clearly indicate that the fences significantly reduced the plume spillage. The decrease in pressure along the edge of the plug was much less than the without-fence configuration. Again, the pressure gradients in this CFD result is very similar to the experimental results shown in Figure 6. The SRPT in Figure 8 show only a slight movement toward the edge of the plug. The fences also resulted in a different plug base flow without the strong recirculation at the outboard edge of the plug base.

Wall Pressures

Without-Fence

Figure 9 presents the experimentally measured wall pressures for the without-fence configuration, normalized by nozzle total pressure. A high density of static pressures were measured on the centerline and a less dense array were measured at eight spanwise locations. Note that the centerline pressure measurements extended upstream (to the left of 0 in Figure 9) on the lower wall of the internal expansion. The measured pressures show a decreasing wall pressure toward the edge of the plug.

Figure 10 presents the corresponding plot from the CFD results. The overall character agrees well with the experimental data shown in Figure 9. It will be shown in subsequent plots that the agreement at each spanwise location is good. Both Figures 9 and 10 indicate that effect of the plume spillage was seen as far inboard as the 70% span pressure profile.

Figure 11a compares the experimental and CFD normalized wall pressures on the plug centerline. The CFD agrees quite well with the experimental data. Figures 11b through 11i compare the normalized experimental and CFD pressures at each spanwise location. In these figures, the experimental data at the plug centerline is included the magnitude to which the plume spillage is affecting the local wall pressure. The CFD exhibits good agreement with the experimental data at each spanwise location. The pressure profiles at 23% span and 47% span are similar to the centerline profile and. Moving outward, the 70% span profile, with a slight decrease in pressure, is the first to show an affect of the plume spillage. Each subsequent profiles shows a further decrease due to plume spillage.

With-Fence

Figure 12 presents the normalized wall pressures for the with-fence configuration as calculated by the CFD at NPR 116. Comparing this figure with 10, the corresponding without-fence wall pressures, two observations about the effect of the fences can be made. First, the profiles at the centerline, 23% span and 47% span were unaffected by the addition of the fences. Second, the fences resulted in higher wall pressures on the outer profiles; 70% span to 97% span. The magnitude of the increased pressure is illustrated in Figures 13a through 13f.

In Figures 13a through 13f, the CFD results at NPR 116 are compared to the experimental data recorded at NPR 110. At each spanwise location, the with-fence wall pressures were higher than the without-fence configuration. The difference was only slight at the 70% span profile but quite dramatic at the outer locations. With the exception of one axial station as indicated in Figures 13b, c, and d, the CFD results agree well with the experimental data.

Plug Base Pressure

Figure 14 presents the plug base pressure at y=0 from the plug centerline outward for both fence configurations. Again, the experimental data for the without-fence configuration is at NPR 116 while the with-fence configuration is at NPR 110. The CFD results for both configurations are at NPR 116. The average plug base pressures are presented in Table 1. In calculating the experimental average plug base pressure profile shown for y=0 was assumed to exist over the entire height of the plug base. For the CFD average plug base pressure, the three dimensional pressure distribution was integrated.

Experiment	Ambient Pressure, P/P_c	Average Base Pressure, P/P_c	Difference from Ambient
Without-Fence	8.65e-3	8.2e-3	-4.8%
With-Fence	9.1e-3	7.4e-3	-18.1%

CFD Results	Ambient Pressure, P/P_c	Average Base Pressure, P/P_c	Difference from Ambient	Difference from Experiment
Without-Fence	8.65e-3	5.87e-3	-32.1%	-28.4%
With-Fence	8.65e-3	6.04e-3	-30.2%	-18.4%

Table 1. Plug Base Pressure Normalized by Total Pressure (P/P_c), Experiment Top, CFD Bottom.

Without-Fence

The experimental average plug base pressures for the without-fence configuration was approximately 4.8% below ambient with a distinctive low pressure region near the edge of the base. The CFD average base pressure was 32.1% below ambient. Relative to the experimental average base pressure the CFD average was 28.4% low. The CFD results do, however, capture the spanwise trend of the experimental base pressures. The magnitude of this error in base pressure is typical for this CFD tool with extended k-ε turbulence model.

With-Fence

The experimental data for the with-fence configuration had a pressure distribution similar to the without-fence configuration. However, the fences reduced the average base pressure further to 18.1% below ambient. The CFD average base pressure was 30.2% below ambient. Again, the general character of the base pressure distribution was capture by the CFD. Relative to the experimental average base pressure the CFD average base pressure for the with-fence configuration improved a bit to 18.4% low. If the difference in ambient pressure is compensated for by scaling the CFD average base pressure by the ratio of the ambient pressure the CFD would be 6.35e-3 P/P_c or 14.1% below the test data.

One trend not captured by the CFD is that the experiment indicated the fences decreased the plug base pressure slightly. This decrease represents about a 0.2% decrease in nozzle thrust efficiency. The CFD results indicate a very small positive increment to plug base pressure that would result in a 0.03% gain in nozzle thrust efficiency.

Assessment of Nozzle Performance

Without-Fence

Thrust was not measured in the experimental campaign. However, because the CFD matched the experimental data so well, the CFD can be used to determine the experimental nozzle efficiency. Nozzle efficiency was calculated as

$$\text{efficiency} = \text{thrust}/\text{thrust}_{ideal}$$

where thrust_{ideal} is that thrust a nozzle should produce at a given NPR.

The efficiency of the nozzle, as calculated in the CFD, is presented first and then an estimate of the experimental nozzle is made. Integrating the CFD solution for net thrust produced a nozzle thrust efficiency of 97.60%. Individual losses in nozzle thrust can be broken down as follows.

- 0.64 point, in thruster
- +0.11 point, cowl pressurization
- 0.25 point, skin friction on plug
- 0.45 point, 'drag' on plug base
- 1.08 point, plume spillage off the plug

The losses in the thruster were due to non-ideal expansion and internal skin friction. The pressurization of the aft facing areas above the thruster and just outboard of the plug added 0.11 point of nozzle efficiency. The skin friction on the plug accounted for a quarter point loss. The drag loss on the plug base was due to local pressure being less than ambient.

The loss due to plume spillage was calculated by comparing the three dimensional distribution of plug pressure to that at the centerline (or two dimensional) of the plug. Integrating the differences between the two and three dimensional pressure distributions over the plug area produced an estimate of the spillage loss as 1.08 points of efficiency.

Note that the integrated nozzle thrust was calculated as 97.60% efficiency (2.4% in losses), while the above losses sum to 2.31 points. The 0.09 point difference is most likely due to the technique used to assess the spillage losses.

As shown in the figures the CFD wall pressures agreed well on the plug and up into the thruster. The only significant difference was on the plug base. The nozzle efficiency from the CFD can be used to estimate the experimental hardware nozzle efficiency by correcting for difference in plug base force. The experimental plug base pressures result in a drag loss of 0.07 points of nozzle efficiency. This is a relative gain of 0.38 point over the 0.45 point loss in the CFD. Therefore, the experimental hardware's nozzle efficiency, for the without-fence configuration, is estimated as 97.98%.

With-Fence

Integrating the CFD solution for the with-fence configuration for net thrust produced a nozzle thrust efficiency of 98.32%. This gain of 0.72 points of efficiency relative to the without-fence configuration was almost entirely due to the reduced spillage off the plug. Individual losses in nozzle thrust can be broken down as follows.

- 0.64 point, in thruster
- 0.03 point, cowl pressurization
- 0.25 point, skin friction on plug and fence
- 0.42 point, 'drag' on plug base
- 0.23 point, three dimensional effects on the plug

The fences had no effect on the losses in the thruster. The fences did cause the aft facing areas above and outboard of the plug to produce a small drag term as opposed to the small thrust term for the without-fence configuration. The skin friction drag on the plug was increased slightly by the fence's presence. The skin friction drag on the fences was also small. Combined, the skin fiction drag term did not increase sufficiently to appear in the two digit accuracy of the loss terms. As mentioned previously, the fences slightly reduced the loss due to drag on the plug base.

As shown in the plots of plug pressure for the with-fence CFD solution, there was still a slight decrease in pressure toward the edge of the plug. The thrust loss due to this three dimensional effect were assessed the same way the plume spillage losses were for the without-fence configuration. Integrating the differences between the two and three dimensional pressure distributions over the plug area for the with-fence configuration produced an estimated loss of 0.23 points of efficiency.

Note that the above losses sum to 1.57 points while the integrated nozzle efficiency was 98.32% or 1.68 points in losses. The 0.11 point difference in losses is most likely due to the technique used to assess the three dimensional pressure distribution losses.

Again, the CFD results for plug base pressure were in error. To estimate the nozzle efficiency of experimental nozzle with fences, the experimental base pressures were used. Because the experiment and the CFD had slightly different ambient pressure, the average experimental plug base pressures were first scaled by the ratio of the ambient pressure to be representative of NPR 116 base pressures. This scaled average plug base pressure, P/P_c=7.02e-3, would produce a drag loss equal to 0.26 points of efficiency. This loss is 0.16 points less than the CFD base drag loss. Therefore, for NPR 116, it is estimated that the experimental nozzle efficiency would be 98.48%.

Comparing this estimate of 98.48% for the experimental hardware for the with-fence configuration to the 97.98% estimate for the without configuration indicated that fences provided a half point increase in nozzle efficiency.

Conclusions

A new design approach based on the method of characteristics was used to design a linear plug nozzle in which the non-uniform primary expansion exit profile is taken into account in the plug contour design. This design approach was validated by means of numerical and experimental work.

In general the results of the CFD analysis agreed well with the experimental results. The plug pressure profiles for both the without-fence and with-fence configurations were well captured by the CFD. The three dimensional effects due to lateral expansion, for the without-fence configuration, were well captured. For the with-fence configuration, the reduced lateral expansion and minor three dimensional effects of expansion were also well captured. The CFD calculated plug base pressure 14 to 28% below the experimental data. The general shape of the plug base pressure gradient was captured. However, the trend of decreased plug base pressure with the addition of fences was not captured.

The CFD results were used to estimate the efficiency of the LION test hardware at NPR 116. Without side wall fences the nozzle was 97.98 % efficient and with side wall fences it was 98.48% efficient. The plug side wall fences provided one-half point gain in nozzle efficiency.

Outlook

Within Europe, the research on linear plug nozzles is currently continued within LPNI, the successor of the LION program. LPNI is funded through the European Space Agency ESA ESTEC, with the following partners involved: EADS Space Transportation (acting as prime), Snecma Moteurs, University of Dresden, University of Delft, and University of Rome. The program started at the end of 2001, and will close-out by the end of 2003.
The key technical objectives are:

- Experimental and numerical assessment of thrust vector control efficiency of the linear plug concept
- Assess a new round-to-square plug module design approach
- Optimization of truncated linear plug contour for maximum thrust
- Develop a full-scale engine plug design
- Integration study of plug engine boat-tail(cowl)

Acknowledgements

The European work within EADS Space Transportation (formerly Astrium Space Infrastructure) was partly financed by the German National Program LION, The authors acknowledge H.-D. Speckmann, DLR Bonn, for the support. The Program has recently been extended towards funding through ESA ESTEC within the frame of a TRP, the authors here acknowledge R. Schwane for the support, and the various partners from Snecma Moteurs (G. Fratacci), TU Delft (M. Wisse), and Univ. of Rome (M. Onofri). For the dedicated experimental effort the authors especially acknowledge S. Niebergall from TU Dresden/HWK Merkes.

References

[1] Hagemann, G., Immich, H., and Dumnov, G., "Critical Assessment of the Linear Plug Nozzle Concept", AIAA Paper 2001-3683, July 2001.

[2] Hagemann, G., Schwane, R. , Reijasse, Ph., and Ruf, J., "NATO RTO WG 10: CFD Results of Plug Nozzle Test Cases", AIAA Paper 2002-4036, July 2002.

[3] Wang, T.-S. and Chen, Y.-S., "Unified Navier-Stokes Flowfield and Performance Analysis of Liquid Rocket Engines," Journal of Propulsion and Power, Vol. 9, No. 5, Sept-Oct 1993, pp.678-685.

[4] Chen, Y.-S., Liaw, P., Shang, H.-M. and Chen, C. P., "Numerical Analysis of Complex Internal and External Viscous Flows with a Second-Order Pressure-Based Method," AIAA Paper 93-2966, July 1993.

[5] Chen, Y.-S. and Kim S. W., "Computation of Turbulent Flows Using an Extended κ-ε Turbulence Closure Model," NASA CR-179204, Oct. 1987.

[6] Chen, Y.-S., Cheng, G. C. and Farmer, R. C., "Reacting and Non-Reacting Flow Simulation for Film Cooling in 2-D Supersonic Flows," AIAA Paper 92-3602, July 1992.

[7] Liakopouls, A., "Explicit Representations of the Complete Velocity Profile in a Turbulent Boundary Layer," AIAA Journal, Vol. 22, No. 6, Jan. 1984, pp. 844-846.

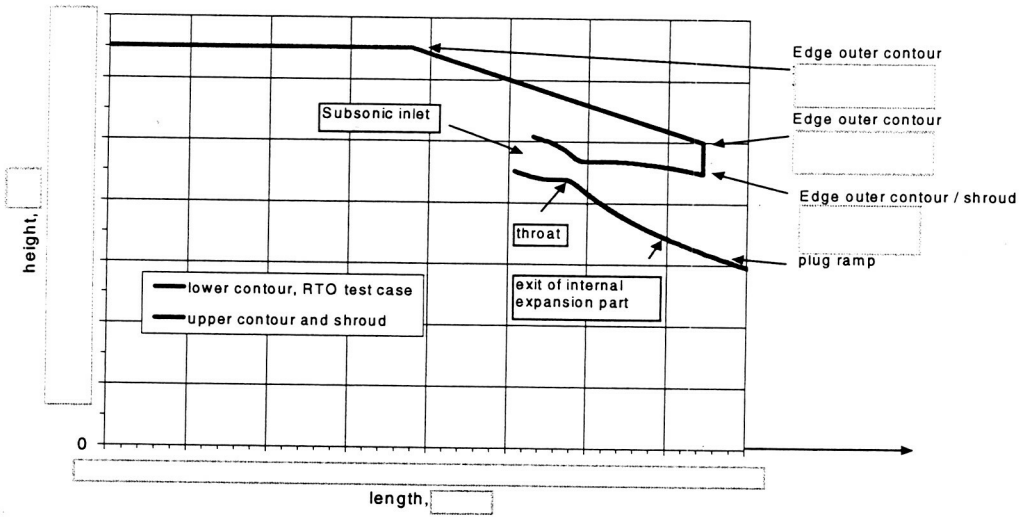

Figure 1. Sketch of LION Plug Model.

Figure 2: LION Test Hardware Mounted in Wind Tunnel of TU Dresden, HWK Merkers.

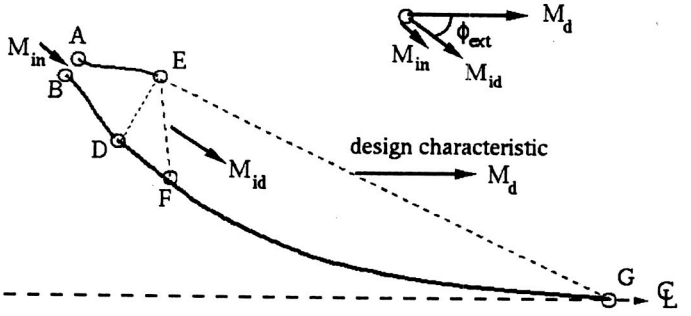

Figure 3: Linear Plug Design with a Combined Internal and External Expansion. Internal Expansion in Symmetric Cell Nozzle.

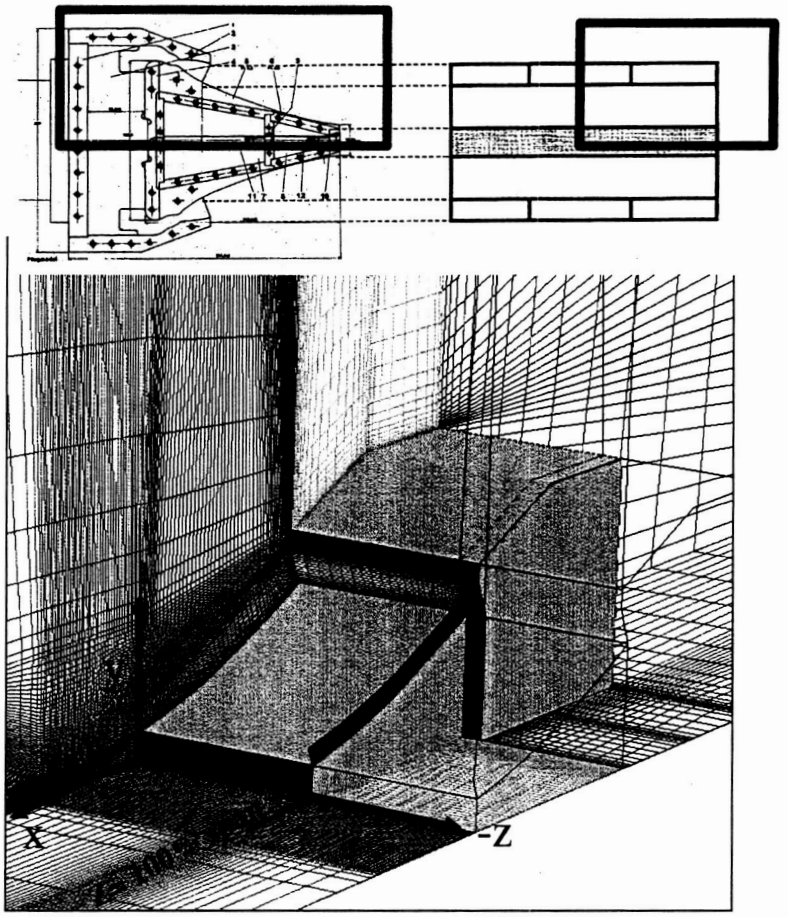

Figure 4. Computational Mesh for External Domain. Every Other Node is Shown.

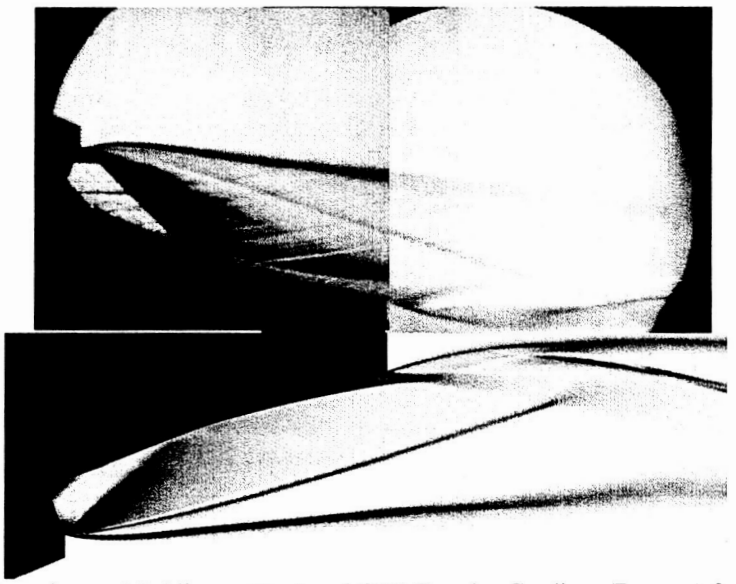

Figure 5. Experimental Schlieren (Top) and CFD Density Gradient (Bottom) for NPR 116.

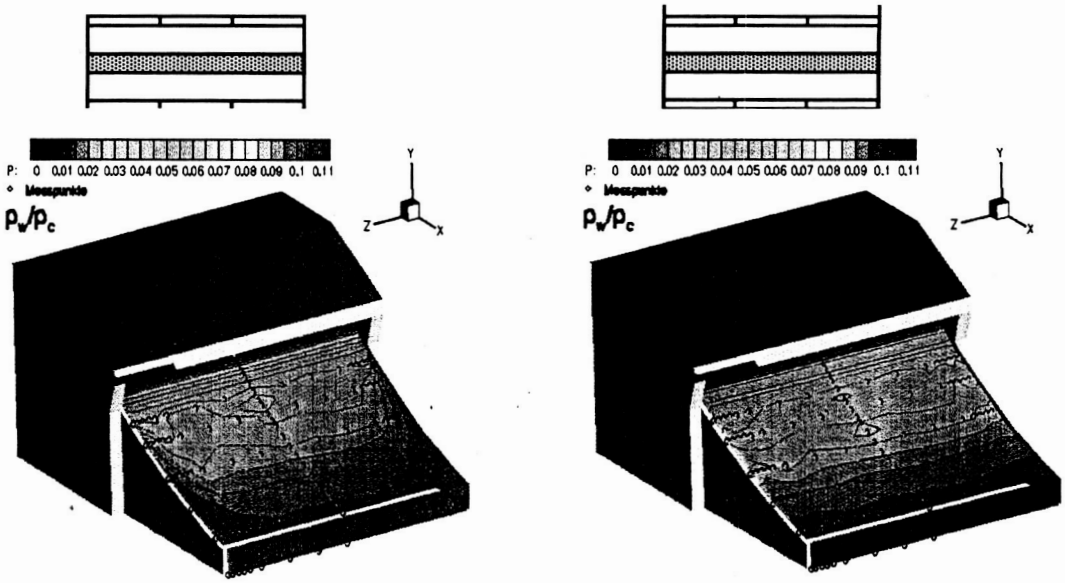

Figure 6: Experimental Plug Wall Pressure Distribution for Configuration without Side-Fence (left), and with Side Fence (right).

Figure 7. CFD Flow Visualization for NPR 116 without-Fences.

Figure 8. CFD Flow Visualization for NPR 116 with-Fences.

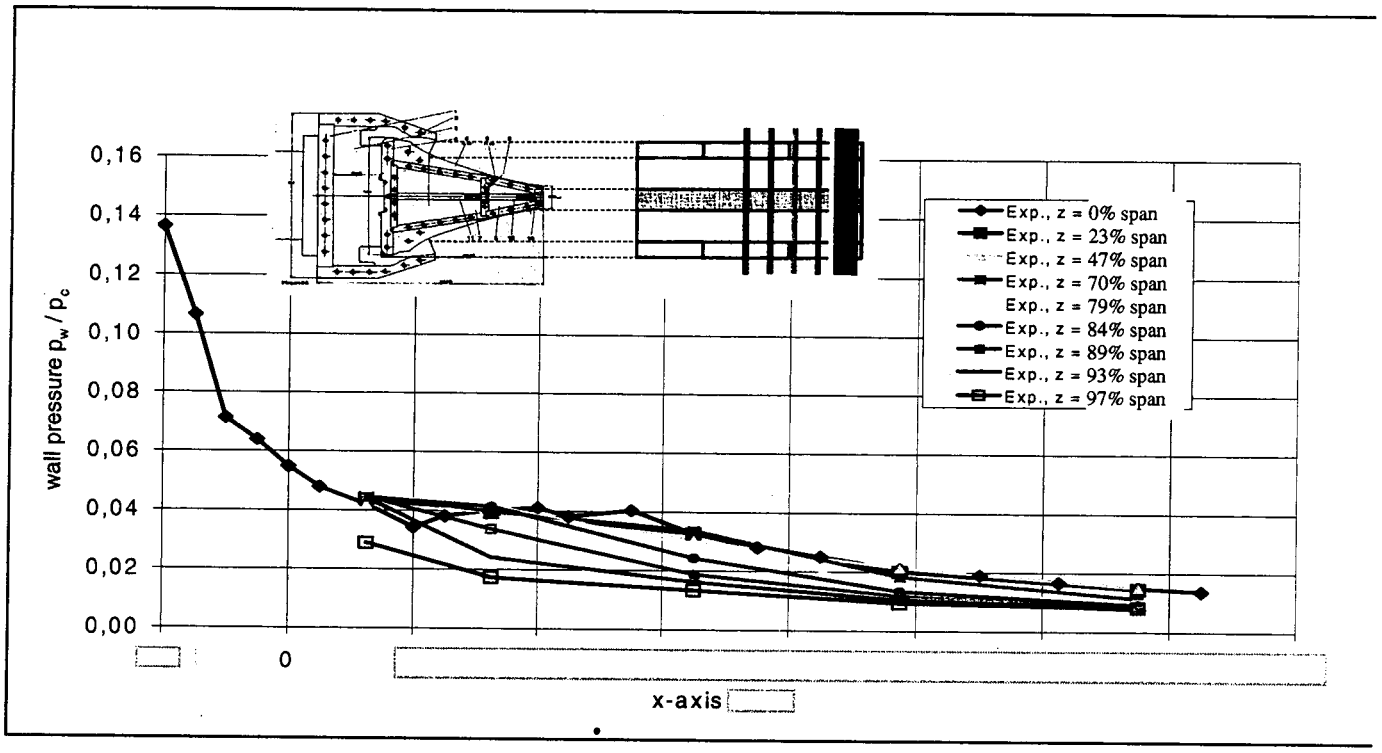

Figure 9. Experimental Spanwise Distribution of Plug Pressure for NPR 110.

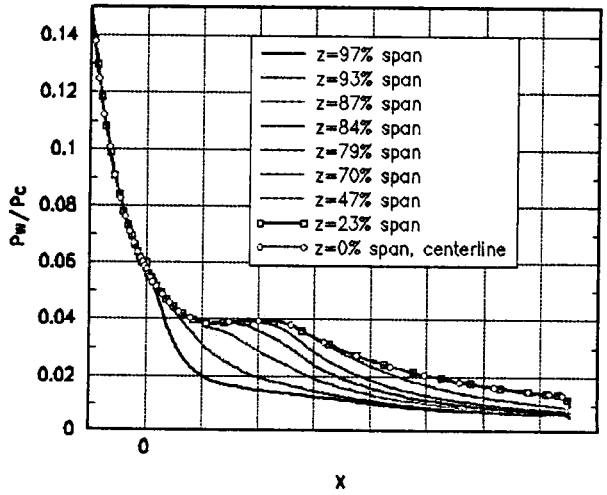

Figure 10. CFD Spanwise Distribution of Wall Pressure for NPR 116 without-Fences.

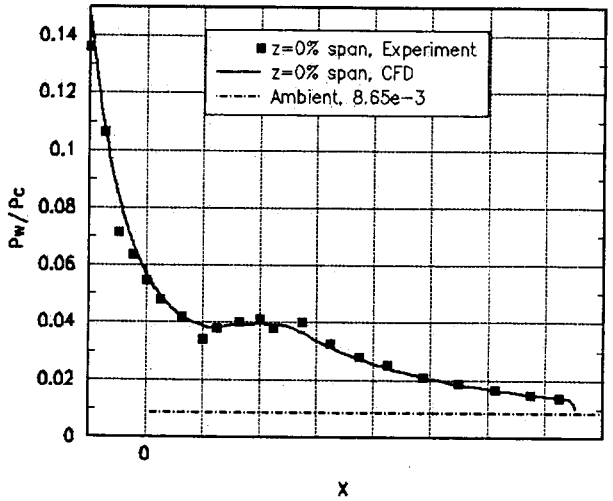

Figure 11a. NPR 116 Experimental and CFD Wall Pressures at Z=0, Centerline.

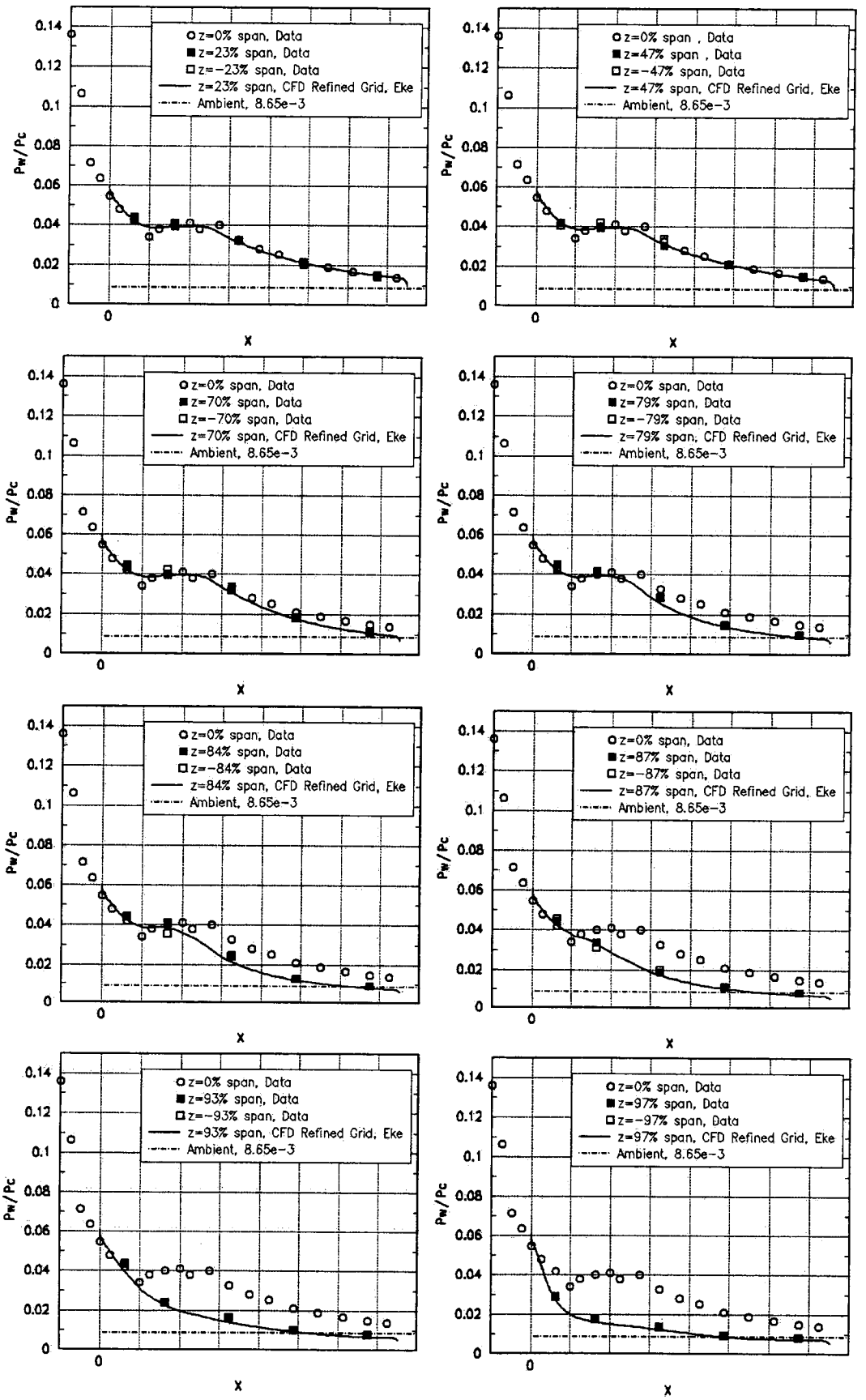

Figure 11b (Top, Left) Through 11i (Bottom Right); Normalized Experimental and CFD Wall Pressure at Each Spanwise Location for NPR 116 with out Fences

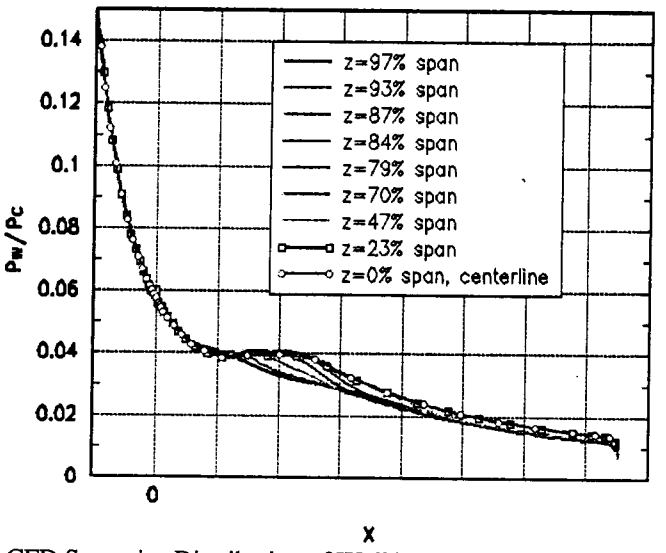

Figure 12. CFD Spanwise Distribution of Wall Pressure for NPR 116 with-Fences.

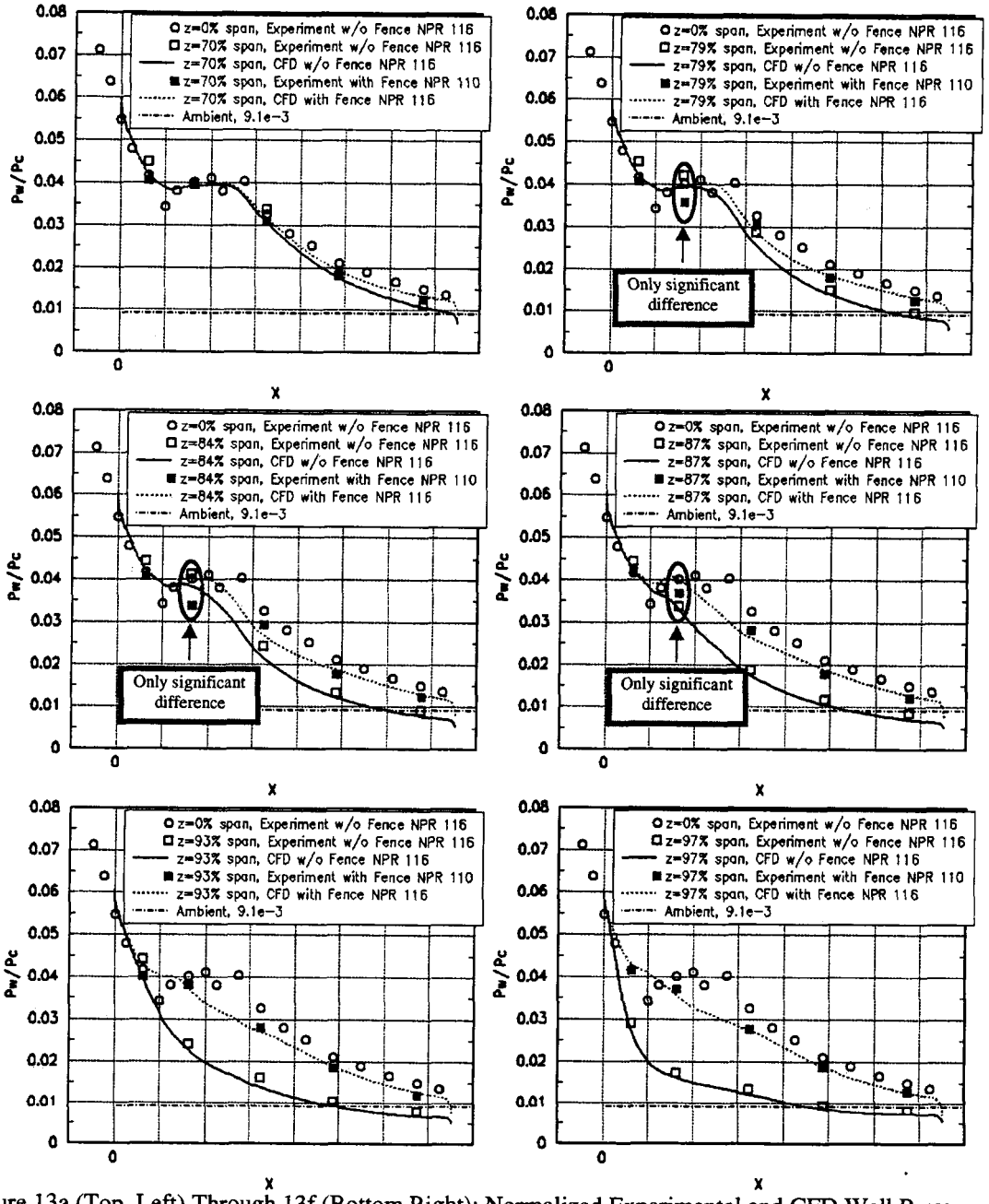

Figure 13a (Top, Left) Through 13f (Bottom Right); Normalized Experimental and CFD Wall Pressure at Each Spanwise Location for NPR116 with-Fences

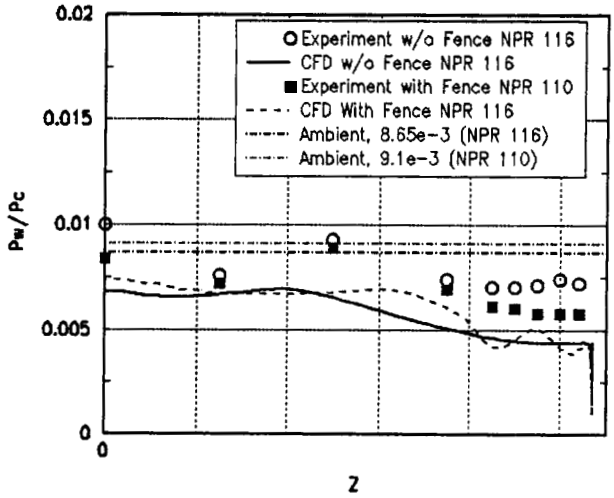

Figure 14. Plug Base Pressure; NPR 110 Experiment, NPR 116 CFD.